Period doubling scenario in low-dimensional models for the regularized cavity flow.

A. Meseguer, F. Marquès, J. Sánchez
Dep. Física Aplicada, Universitat Politècnica de Catalunya,
08034 Barcelona, Spain.

October 6, 1995

Abstract

We present a four-dimensional model for the regularized cavity flow, obtained by truncating a dynamical system of amplitudes for the velocity field. A spectral Legendre-tau scheme in primitive variables has been used in order to obtain this system. This low-dimensional model exhibits a route to chaos via a period doubling cascade. The period doublings and the chaotic region (for moderate Reynolds number) are analysed in detail.

Key words: Navier-Stokes equations; period doubling cascade; strange attractors.

1 Introduction.

Low-dimensional analysis of fluid systems are of interest in order to capture the essential features of their behaviour. Many fluid dynamics problems have been analysed from this point of view (see Lorenz [1] or Boldrighini [2], for example). Of course, the results obtained from these models may not be realistic due to the excessive truncation of the equations. On the other hand, this kind of models usually provide us relevant information about the core dynamics that governs the fluid motion.

The regularized driven cavity flow is perhaps one of the most well known problems in computational fluid dynamics. The simplicity of the problem makes it possible to test numerical schemes of integration for the Navier-Stokes equations of incompressible fluids. This problem has already been solved numerically by many authors (see Shien [3] and [4], for example). In particular, Shien [3] has analysed the behaviour of the system for a wide range of Reynolds numbers. For Reynolds numbers below $Re = 10.000$ the solution is stationary but a Hopf bifurcation occurs at a critical Reynolds number in the range [10.000, 10.500]. For $Re = 15.500$ the flow lost its time periodicity and the numerical evidence suggests that it became quasiperiodic. One would expect that further increase of the Reynolds number would lead to a turbulent flow.

In this paper we introduce a low-dimensional analysis for the regularized driven cavity flow. We use a spectral Legendre-tau scheme in primitive variables in order to obtain a dynamical system of amplitudes for the velocity field. By truncating the system up to order four, a relatively simple system of ordinary differential equations is obtained. Its analysis is the main subject of this paper. We have found different stationary solutions at low Reynolds number, but only one of them is stable. This solution loses stability at a Hopf bifurcation, and suffers a cascade of period doubling bifurcations. We have computed these period doublings with suitable accuracy by using a method based on the first variational equations for the Poincaré map.

For the four-dimensional system we obtain a period doubling scenario in the Reynolds interval [503.26, 512.468]. This period doubling cascade verifies Feigenbaum's universality. Beyond $Re = 512.468$ the system presents chaotic behaviour. This is reflected in the Liapunov exponents analysis and in the Fourier spectra of the time evolution. Also, the structure of the Poincaré section of the attractor presents fractal features.

The paper is organized as follows. In Section 2 we present the mathematical formulation for the problem. In Section 3 we analyse the four-dimensional model, and introduce a numerical method in order to obtain the period doubling bifurcations with great accuracy; the resulting cascade is presented in detail. We analyse the behaviour of the Liapunov exponents as a function of the Reynolds number in order to analyse the chaotic zone. Inside this region, periodic windows are obtained. We also present the results of the Fourier spectra from time integrations of the dynamical system for different regions. Finally, a Poincaré section of the strange attractor is visualized in order to analyse its self-similarity structure, typical of this kind of object.

2 The regularized driven cavity flow.

2.1 Mathematical setting.

We consider the adimensionalized Navier-Stokes equations for incompressible fluids:

$$\partial_t \mathbf{v} + (\mathbf{v}\cdot\nabla)\mathbf{v} = -\nabla p + \Delta \mathbf{v} \quad , \quad \nabla\cdot\mathbf{v} = 0 \tag{1}$$

In order to develop a weighted residuals scheme we will work with two different function spaces. Let H_d be the projection space of test functions:

$$H_d = \{\tilde{\phi} \in L^2(\Omega),\ \nabla\cdot\tilde{\phi} = 0,\ \tilde{\phi}\cdot\hat{n}\ |_{\partial\Omega} = 0\} \tag{2}$$

where $\hat{n}$ is the unit normal to $\partial\Omega$, and let H_s be the space of divergence-free functions:

$$H_s = \{\hat{\phi} \in L^2(\Omega),\ \vec{\nabla}\cdot\hat{\phi} = 0\} \tag{3}$$

The weak form of problem (1) will be

$$< \tilde{\phi} \mid \partial_t \mathbf{v} + (\mathbf{v}\cdot\nabla)\mathbf{v} - \Delta\mathbf{v} >= 0 \quad , \quad \forall\tilde{\phi}\in H_d,\ \mathbf{v}\in H_s \tag{4}$$

In the previous equation $< \cdot \mid \cdot >$ is the standard Hermitian product between functions. The pressure term $< \tilde{\phi} \mid \nabla p >$ vanishes for all $\tilde{\phi} \in H_d$ (see Temam [5]).

The regularized driven cavity flow consists of a two-dimensional square box filled with an incompressible fluid, whose velocity is given on one box side, and zero on the remaining ones. We adimensionalize the variables using $L_0/2$, $L_0/2\nu$ as the unit length and velocity; L_0 is the side length of the box. The fluid domain is $\Omega = [-1,1]\times[-1,1]$, and we will use Cartesian coordinates (x,y). The boundary conditions are:

$$\vec{v}(\pm 1, y) = (0,0), \quad \vec{v}(x,-1) = (0,0), \quad \vec{v}(x,1) = \vec{v}_\Gamma = (R(x^2-1)^2, 0) \tag{5}$$

where R is the Reynolds number $R = L_0 v_0/2\nu$ (which differs by a factor $\frac{1}{2}$ from the Reynolds number considered by other authors), and v_0 is the maximum of the imposed velocity on the side $y=1$. We have taken a regularized velocity profile giving a continuous boundary condition on $\partial\Omega$ (see Peyret [6], for example).

2.2 Selection of H_d, H_s .

Both spaces will be spanned by solenoidal functions

$$H_d = \text{Span} < \tilde{\phi}_{pq} > \quad , \quad H_s = \text{Span} < \phi_{mn} > \tag{6}$$

of the form

$$\tilde{\phi}_{pq}(x,y) = \begin{pmatrix} -\tilde{f}_p(x)\tilde{g}_q'(y) \\ \tilde{f}_p'(x)\tilde{g}_q(y) \end{pmatrix} \quad , \quad \phi_{mn}(x,y) = \begin{pmatrix} -f_m(x)g_n'(y) \\ f_m'(x)g_n(y) \end{pmatrix} \tag{7}$$

where $'$ means derivative. These vectorial functions satisfy the divergence–free condition and are a base of the Hilbert space H_s. Now the velocity field is of the form:

$$\mathbf{v}(x,y,t) = \sum_{m=0}^{M}\sum_{n=0}^{N} a_{mn}(t)\phi_{mn}(x,y) \tag{8}$$

We suppose that $\tilde{\phi}_{pq}$ and ϕ_{mn} are continuous and differentiable vector fields defined in Ω such that the normal component of $\tilde{\phi}_{pq}$ vanishes on the boundary $\partial\Omega$ of the domain:

$$\tilde{\phi}\cdot\hat{n} = 0 \tag{9}$$

The selection criteria of the set of functions $\tilde{\phi}_{pq}$ and ϕ_{mn} depend on the geometry of the problem and the boundary conditions. In fact, these functions will be built up using suitable orthogonal polynomials (see Canuto [7] or Moser [8] for a detailed discussion). The functions $\tilde{f}_p$ and $\tilde{g}_q$ contain three factors. Two of them are the corresponding orthogonal polynomial and its weight function ($\omega(x) = 1$ for Legendre polynomials, $\omega(x) = (1-x^2)^{-1/2}$ for Tchebychev polynomials, etc.). The third factor is a suitable low-order polynomial in order to verify the boundary condition (9).

$$\tilde{f}_p(x) = Q_p(x)\omega_Q(x)q(x) \tag{10}$$

(and the same for $\tilde{g}_q(y)$). The weight function is included in order to simplify further calculations.

The structure of ϕ_{mn} is the same as that of $\tilde{\phi}_{pq}$, the only difference being that $f_m(x)$ does not contain the weight function. The low-order polynomial $q(x)$ is not necessary because the function ϕ_{mn} does not need to verify the condition (9). But the condition (9) is part of the boundary conditions for the velocity field (5), therefore if we include $q(x)$ in ϕ_{mn} the normal component of (5) will be satisfied automatically. We have chosen Legendre polynomials in this work, therefore $\omega(x) = 1$ and H_d and H_s coincide, giving the classical Galerkin method. If we had used Chebishev polynomials, these spaces would not have been the same, and we would be dealing with the generalized Petrov-Galerkin method. We take the f and g functions as

$$\tilde{f}_p(x) = f_p(x) = (x^2 - 1)^2 P_p(x) \tag{11}$$

$$\tilde{g}_q(y) = g_q(y) = (y^2 - 1) P_q(y) \tag{12}$$

where P_p is the p^{th}-order Legendre polynomial. Thanks to the factors $(x^2-1)^2$ and y^2-1 the boundary conditions (5) are satisfied, except for the tangential component on $y = \pm 1$. This remaining boundary condition will be set by the tau method.

2.3 The equations.

Substituting the spectral approximation (8) into the weak form of the Navier-Stokes equation (4) we obtain a system of ODE for the amplitudes $a_{mn}(t)$:

$$\bar{A}^{mn}_{pq} \dot{a}_{mn} = \bar{B}^{mn}_{pq} a_{mn} - \bar{S}^{mnjk}_{pq} a_{mn} a_{jk} \tag{13}$$

where we have used the Einstein convention of addition with respect to the repeated indexes. The coefficients are:

$$\bar{A}^{pm}_{qn} =< \phi_{pq} \mid \phi_{mn} > \quad , \quad \bar{B}^{pm}_{qn} =< \phi_{pq} \mid \Delta \phi_{mn} > \tag{14}$$

$$\bar{S}^{pq}_{mnjk} =< \phi_{pq} \mid (\phi_{mn} \cdot \vec{\nabla}) \phi_{jk} > \tag{15}$$

When the remaining boundary conditions are set, the coefficients a_{mn} are no longer independent. In fact we can find $a_{m,N}$, $a_{m,N-1}$ in terms of the remaining $a_{m,n}$, for all m. From (5),

$$a_{m,n} = -\frac{R}{4}\delta_{m,0} - \sum_{k=1}^{[n/2]} a_{m,n-2k} \; ; \qquad n = N,\, N-1 \; ; \quad m = 0 \div M \tag{16}$$

corresponding to the imposed velocity profile $v(x) = R(x^2-1)^2$ on $y = 1$. Our method allows us to work with more complex velocity profiles. For example, the profile $v(x) = Rx(x^2-1)^2$, corresponding to a collision between two opposite horizontal jets, changes the previous equations to:

$$a_{m,n} = -\frac{R}{4}\delta_{m,1} - \sum_{k=1}^{[n/2]} a_{m,n-2k}\ ; \qquad n = N,\ N-1\ ; \quad m = 0 \div M \qquad (17)$$

These relationships between the coefficients will modify the structure of our dynamical system. Substituting (16) in (13) we get

$$A_{pq}^{mn}\dot{a}_{mn} = Rb_{pq} + R^2 c_{pq} + \left(B_{pq}^{mn} + RC_{pq}^{mn}\right) a_{mn} + S_{pq}^{mnij} a_{mn} a_{ij} \qquad (18)$$

where a, b, A, B, C, S are constant tensors, whose expressions can be found in Appendix A. We have written explicitly the dependence on the Reynolds number R. The constant terms independent of a_{mn} are source terms induced by the external forcing, R being a measure of it. The system (18) has $(M+1)\times(N-1)$ independent equations for the amplitudes a_{mn}, $m = 0 \div M$, $n = 0 \div N-2$.

3 A four-dimensional model.

Low-dimensional models can be obtained by truncation of the previous equations at low order. Taking two independent modes in both x and y variables ($M = 1$, $N = 3$), we get a four-dimensional dynamical system for the amplitudes.

$$\begin{pmatrix} \dot{u} \\ \dot{v} \\ \dot{w} \\ \dot{z} \end{pmatrix} = R \begin{pmatrix} -\lambda_1 \\ -\lambda_2 \\ 0 \\ 0 \end{pmatrix} + R^2 \begin{pmatrix} 0 \\ 0 \\ -\lambda_3 \\ -\lambda_4 \end{pmatrix} - \begin{pmatrix} d_1 & 0 & 0 & 0 \\ 0 & d_2 & 0 & 0 \\ 0 & 0 & d_3 & 0 \\ 0 & 0 & 0 & d_4 \end{pmatrix} \begin{pmatrix} u \\ v \\ w \\ z \end{pmatrix} +$$
$$R \begin{pmatrix} 0 & 0 & -\nu_1 & \nu_2 \\ 0 & 0 & -\nu_3 & -\nu_4 \\ -\delta_1 & \delta_2 & 0 & 0 \\ \delta_3 & \delta_4 & 0 & 0 \end{pmatrix} \begin{pmatrix} u \\ v \\ w \\ z \end{pmatrix} + \begin{pmatrix} \rho_1 uz - \rho_2 vw \\ \rho_3 uw - \rho_4 vz \\ \rho_5 wz - \rho_6 uv \\ \rho_7 u^2 + \rho_8 v^2 - \rho_9 w^2 - \rho_{10} z^2 \end{pmatrix} \qquad (19)$$

The coefficients are numerical constants which can be found in Appendix A.

The previous equations are too complicated to find analytical expressions for the stationary points and their dependence on the Reynolds number R.

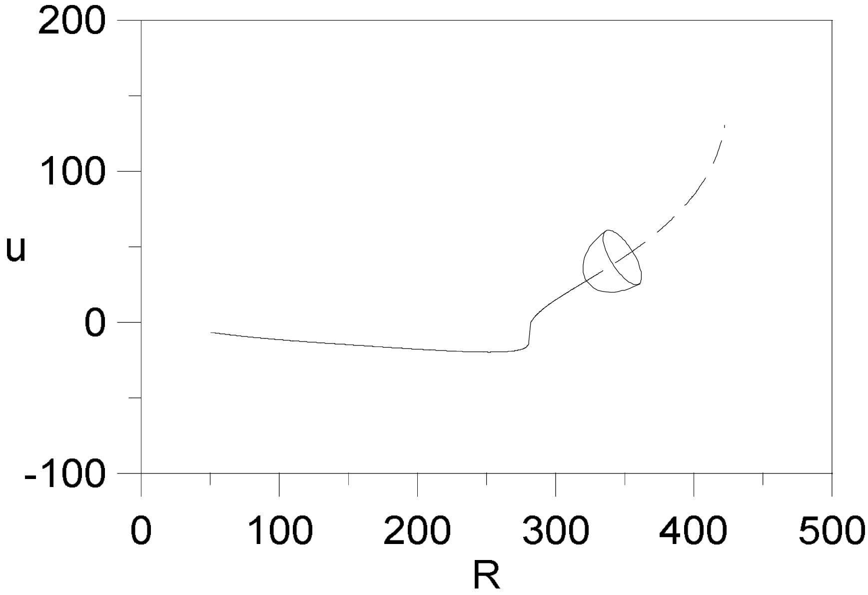

Figure 1: Fixed points as a function of the Reynolds number R. Solid lines means stable, and dashed lines, unstable points. The parabolic shape that emerges from the continuous line represents the periodic orbit generated by the Hopf bifurcation.

Nevertheless, we find the branches numerically by continuation methods; see [9]. The branches are sketched in Figure 1. We have computed the eigenvalues of the Jacobian matrix over every one of the branches as a function of the parameter R. We conclude that only one of them is stable. We will focus our attention on this branch. For values of R less than 321.5 the eigenvalues have negative real part. For $R = 321.5$ one pair of eigenvalues croses the imaginary axis with non-zero imaginary part. Thus, a Hopf bifurcation appears. The orbit generated by this bifurcation is stable over the interval [321.5, 503.26].

3.1 Period doubling scenario. The Newton–variational method.

In order to fix the stability and secondary bifurcations of the periodic orbit γ that appears in the Hopf bifurcation, we have used a Poincaré map. Let Π_0 be a hyperplane transversal to γ in a point $x_0 \in \gamma$. We will write the system (19) as $\dot{x} = f(x, R)$ for the sake of simplicity, and let $\phi(t, x)$ be the solution of this system with x_0 as initial condition ($\phi(0, x) = x$). The equation of Π_0 is $(x - x_0) \cdot \xi = 0$, where ξ satisfies the transversality condition $\xi \cdot f(x_0, R) \neq 0$. The Poincaré map is given by

$$\begin{array}{rccl} P: & \Pi_0 & \longrightarrow & \Pi_0 \\ & x & \longrightarrow & P(x) = \phi(\tau(x), x) \end{array} \quad \text{where} \quad (\phi(\tau(x), x) - x_0) \cdot \xi = 0 \quad (20)$$

The eigenvalues of DP give the stability of the periodic orbit γ. DP is the restriction to Π_0 of the solution of the first variational equation

$$\dot{J} = D_x f(\phi(t, x_0), R) J \quad , \quad J(0) = \mathbf{1}_4 \qquad (21)$$

where $\mathbf{1}_4$ is the identity matrix in $\mathbb{R}^4$. The projection on Π_0 is given by

$$DP = (\mathbf{1}_4 - \frac{f(x_0, R) \otimes \xi}{f(x_0, R) \cdot \xi}) J \mid_{\Pi_0} \qquad (22)$$

DP is a 3×3 matrix.

The method we have termed Newton–variational is an iterative method that gives us simultaneously the periodic orbit, its period and the differential of the corresponding Poincaré map. From an initial point x^k near to γ and an estimate T^k of the period, we integrate the system

$$\begin{array}{lcl} \dot{x} = f(x, R) & , & x(0) = x^k \\ \dot{J} = [D_x f(x, R)] J & , & J(0) = \mathbf{1}_4 \end{array} \qquad (23)$$

Next we refine the period by integrating the dynamical system (23) up to a final time $t = T^{k+1}$ that verifies the cut with the Poincaré section:

$$(\phi(T^{k+1}, x^k) - x^k) \cdot \xi = 0 \qquad (24)$$

This time can be obtained iteratively by linear interpolation or the bisection method. After that, we have a final point $x^{k+1/2}$, the Jacobian matrix and

DP at this time T^{k+1}:

$$\begin{array}{l} x^{k+1/2} = \phi(T^{k+1}, x^k), \quad J^{k+1} = J(T^{k+1}) \\ DP^{k+1} = (\mathbf{1}_4 - \frac{f(x^k;R)\otimes\xi}{f(x^k;R)} \cdot \xi) J^{k+1} \mid_{\Pi_k} \end{array} \tag{25}$$

The last step of the iteration is the corrector Newton process in Π_k:

$$x^{k+1} = x^k + (\mathbf{1}_3 - DP^{k+1})^{-1}(x^{k+1/2} - x^k) \tag{26}$$

The matrix $\mathbf{1}_3 - DP^{k+1}$ must be invertible, i.e., its eigenvalues must be different from 1. But when γ is stable, the eigenvalues have moduli less than 1, and the bifurcations we have found are period doubling ones. The critical eigenvalue croses the unit circle by -1 and the matrix of the Newton method is invertible. For $k \to \infty$, x^k gives a point of the orbit, regardless of whether it is stable or not. T^k and DP gives its period and eigenvalues.

This iterative method is the core of a continuation method in the Reynolds number R. We start with a R value at which γ is stable and obtain the first orbit by time evolution of (19). For a new value of R the iteration begins with a point and the period of the previous orbit; if the orbit suffers a period doubling bifurcation, the new orientative period will be twice the former period.

The vector ξ is constant througout the process, in order to simplify the calculations and always use the same coordinates for Π_0. The transversality to γ is ensured by moving x_0 along the orbit to a point p_γ where the angle between the orbit and the Poincaré Map is maximum:

$$\frac{f(x,R)\cdot\xi}{\|f(x,R)\|\|\xi\|} \leq \frac{f(p_\gamma,R)\cdot\xi}{\|f(p_\gamma;R)\|\|\xi\|} \quad \forall x \in \gamma \tag{27}$$

By gradually varying the Reynolds number R we can determine with a high degree of accuracy (by succesive linear interpolation, for example) the bifurcating values of R. We have found a period doubling cascade, whose first nine period doubling bifurcation values can be seen in Table 1. The table also shows the ratios between the successive bifurcation intervals, defined by:

$$\delta^n = \frac{R^{n+1} - R^n}{R^{n+2} - R^{n+1}} \tag{28}$$

We can observe that these ratios approach Feigenbaum's universal constant $\delta_F = 4.66920160\ldots$. The R^n sequence has an accumulation point at $R^\infty = 512.468014489$.

R_{crit}	δ
R^1=503.26263580	
R^2=507.98889404	δ^1=1.113
R^3=512.23403718	δ^2=23.361
R^4=512.41575610	δ^3=4.3590
R^5=512.45743770	δ^4=5.0208
R^6=512.4657403824	δ^5=4.6436
R^7=512.4675281125	δ^6=4.6773
R^8=512.4679103180	δ^7=4.6689
R^9=512.4679921795	

Table 1: Critical Reynolds numbers R^n and ratios δ^n for the period doubling cascade.

The first one, two, four and eight periodic states are sketched in Figure 2, where we have represented the amplitude z versus the amplitude v.

3.2 Liapunov exponents.

Liapunov exponents give us information about the stability of the orbits and the long-term behaviour of the volume elements in phase space (i.e., contraction and expansion). For our problem we consider again the first order variational dynamical system

$$\begin{array}{lcl} \dot{x} = f(x,R) & , & x(0) = x_0 \\ \dot{J} = [D_x f(x,R)]J & , & J(0) = \mathbf{1}_4 \end{array} \qquad (29)$$

where now x_0 is a point of the orbit or the attractor to be considered, obtained after a suitable transient time integration. At every time we can compute the eigenvalues μ_j of the matrix J. Then, the Liapunov exponents of our dynamical system will be:

$$\lambda_j = \lim_{T\to\infty} \frac{\log \mid \mu_j \mid}{T} \qquad (j = 1,2,3,4) \qquad (30)$$

When the Liapunov exponents are evaluated directly by integrating the first variational equations (29), numerical problems arise. The columns of

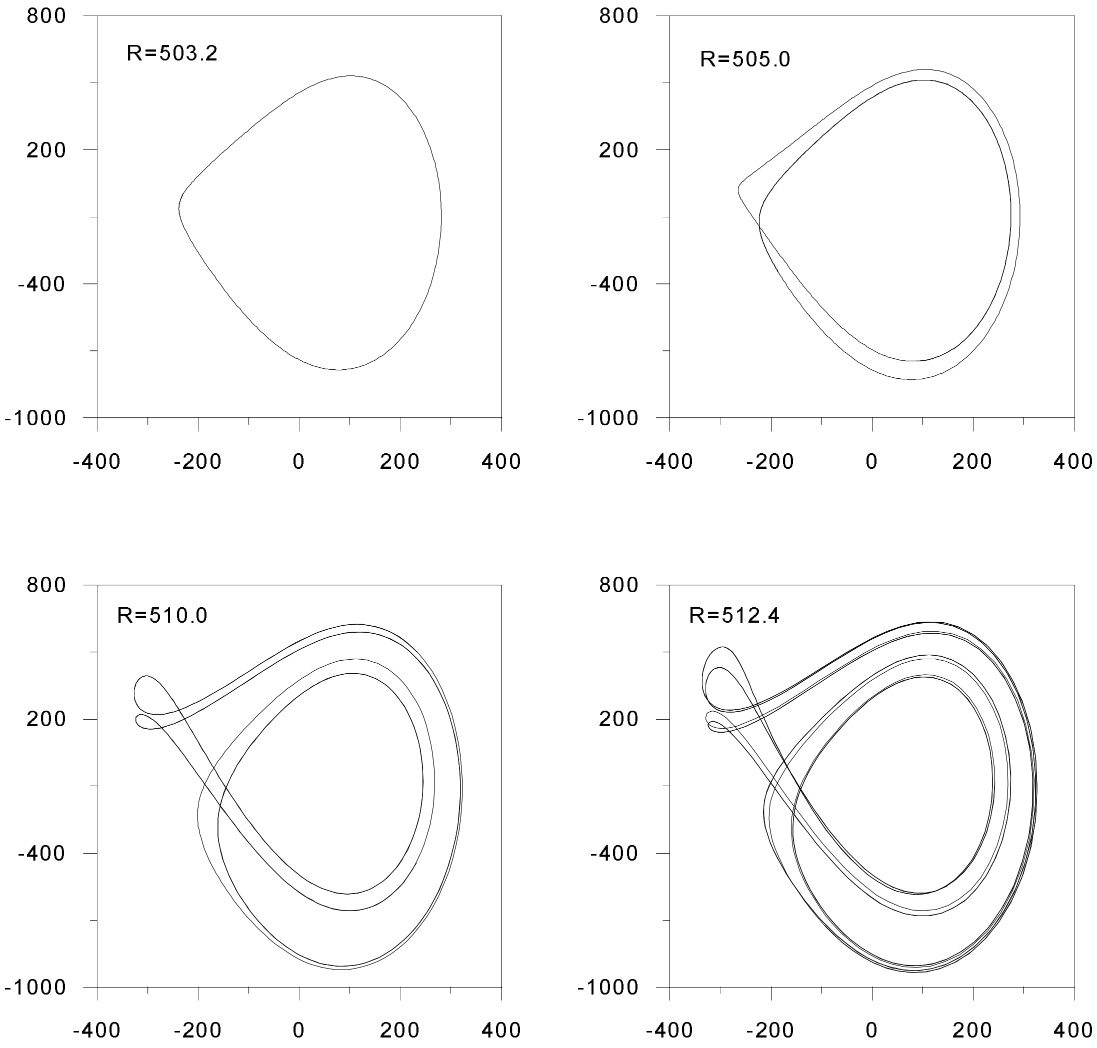

Figure 2: Orbits of the one, two, four and eight periodic states. In the figures the x axis corresponds to the v amplitude and the y axis to the z amplitude.

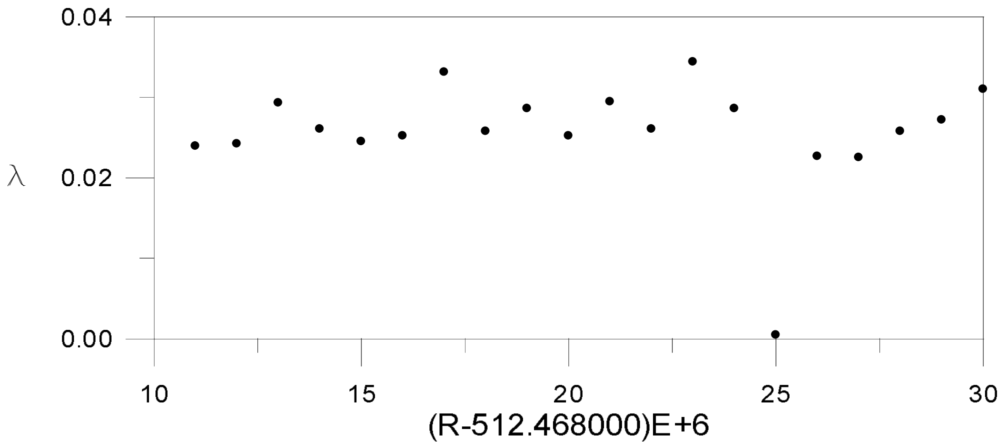

Figure 3: Maximum Liapunov exponent as a function of the Reynolds number R. Note the periodic solution at $R = 512.468025$

$J(t)$ become almost parallel to the direction of the biggest Liapunov exponent, J becomes ill conditioned, and tends to be singular. Furthermore, if some of the Liapunov exponents are greater than zero, overflow problems can occur. Therefore, the previous limit cannot be computed directly. To remedy this problem, we have used the renormalization method of Shimada and Nagashima [10], described in Kubicek [11]. We have computed the Liapunov exponents as a function of the Reynolds number. For the periodic solutions ($R \leq R^{\infty}$) we have a zero exponent and the remaining ones are less than zero, as is well known. The behaviour of the greatest Liapunov exponent for $R > R^{\infty}$ is displayed in Figure 3. Positive values of the exponent correspond to chaotic solutions, and we see that the system is chaotic but presents a window with a periodic stable solution. This behaviour is typical of many dynamical systems that suffer a period doubling cascade. Also, the system exhibits strong hysteresis. Different initial conditions can lead to different solutions, periodic solutions or chaotic solutions.

The strange attractor corresponding to the chaotic zone ($R = 512.5$) is sketched in Figure 4. We have computed a Poincaré section in order to analyse its geometric structure. This section is depicted in Figure 5 for $R = 512.5$. Its self-similarity structure, typical of strange attractors is apparent.

The Fourier spectra for two different Reynolds numbers are shown in

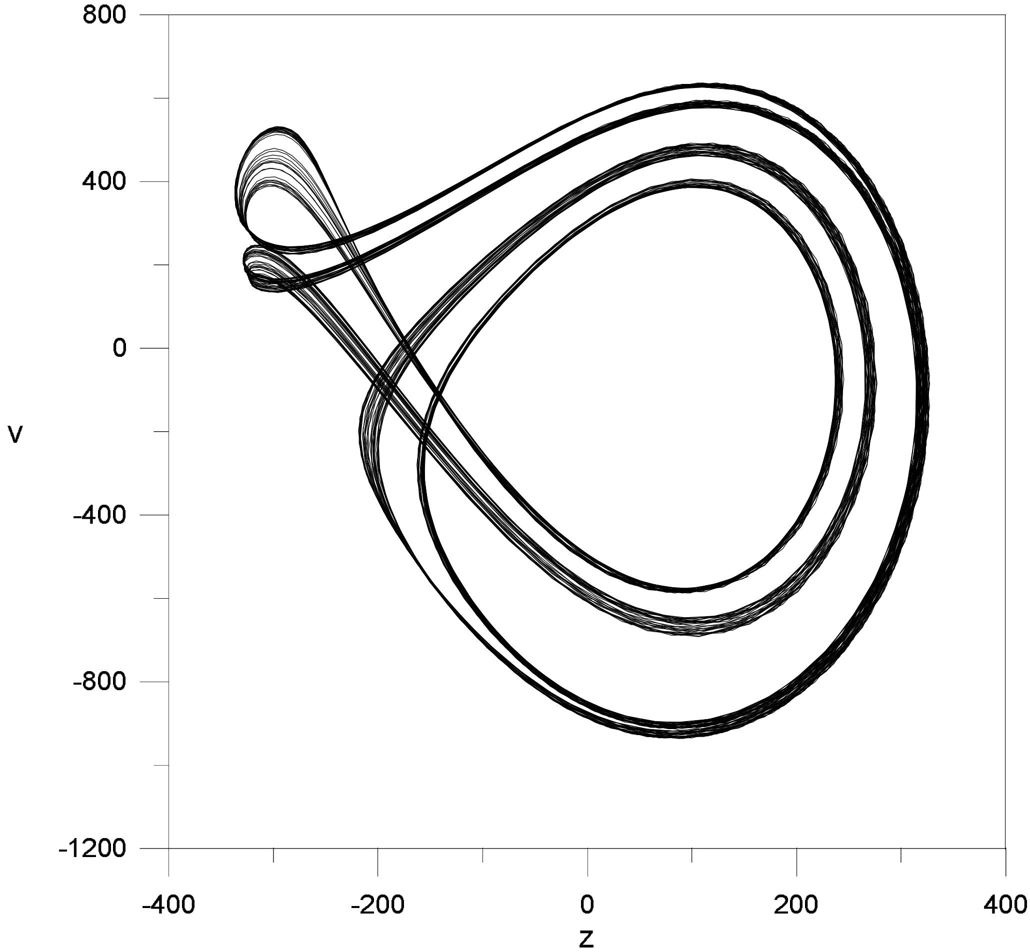

Figure 4: Plot of the strange attractor for $R = 512.5$. Projection into the plane (v,z).

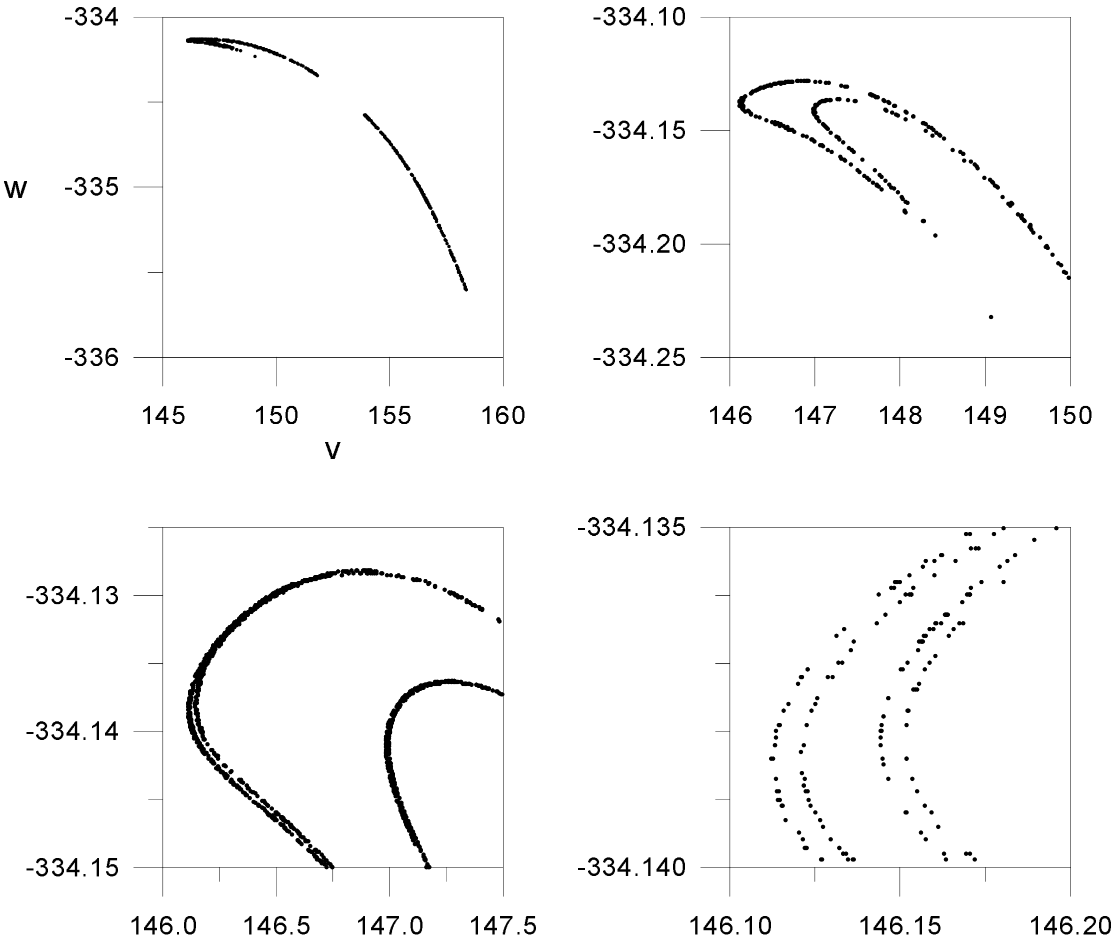

Figure 5: Poincaré section of the strange attractor for $R = 512.5$. The enhanced areas show a self-similar structure. The variables displayed are (v, w)

Figure 6. The first spectrum corresponds to a periodic orbit, and the second one is in the chaotic region. We notice that the former exhibits a broad-band noise, whose level is two or more orders of magnitude higher than in the periodic case. This is a typical signature of chaos. In the chaotic spectrum sharp peaks appear above the level of the noise. Similar types of spectrum have been observed by other authors: Kubicek [11] and Farmer [12]. This type of spectrum is called "phase coherent", and occurs close to unstable limit cycles generated by the sequence of period doubling bifurcations.

If we further increase the Reynolds number the chaotic attractor seems to collapse with the unstable manifold of one of the branches of solutions. This collision produces a destabilization of the attractor. This phenomenon is probably due to the excessive truncation of the model.

In order to check the behaviour of this low-dimensional model, we have obtained a six-dimensional system for the same problem, taking $M = 2$, $N = 3$. The results obtained are very similar. The six-dimensional model also exhibits a period doubling scenario. The bifurcations take place at different Reynolds numbers.

4 Conclusions.

By analysing a four-dimensional model for the regularized cavity flow we find a transition to chaos by means of a period doubling cascade. The period doubling verifies Feigenbaum's universality. After the successive period doubling bifurcations, the system presents a chaotic behaviour. This is reflected in the Liapunov exponents and in the Fourier spectra of the time integrations of the dynamical system. A six-dimensional model is obtained in order to check the results with the previous one. In both cases, the qualitative phenomena are essentially the same. These results suggest that the regularized cavity flow may also exhibit a period doubling cascade as a route to turbulence. The numerical evidence for high Reynolds numbers is not conclusive, and it would be compatible with the results presented in the present work.

Acknowledgements.

This work was supported by the Dirección General de Investigación Científica y Técnica (DGICYT), under grant PB91/0595.

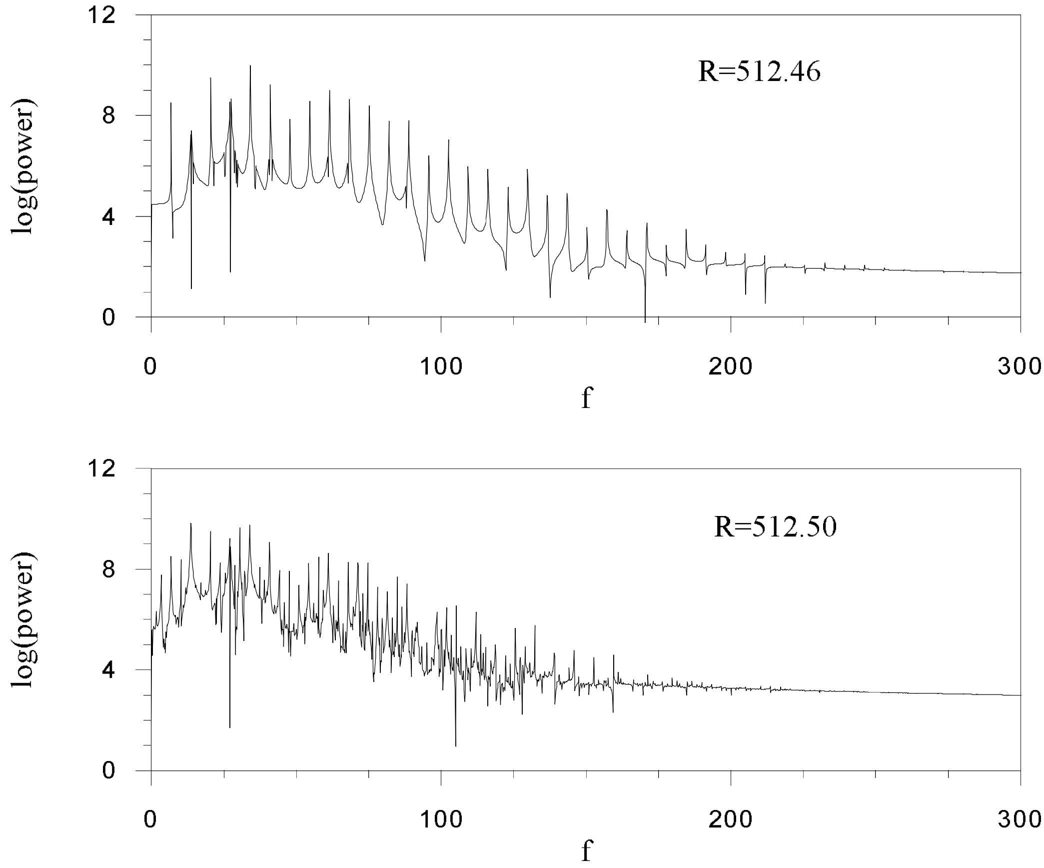

Figure 6: Fourier spectra for a periodic solution ($R = 512.46$) and a chaotic solution ($R = 512.50$).

A Appendix.

The values of the numerical constants that appear in the equations (19) are:

$$
\begin{array}{llll}
\lambda_1 = 133/64 & \lambda_2 = 573/80 & \lambda_3 = 991/20592 & \lambda_4 = 73/5720 \\
\nu_1 = 23/2904 & \nu_2 = 1615/113256 & \nu_3 = 703/15730 & \nu_4 = 685/9438 \\
d_1 = 483/32 & d_2 = 267/8 & d_3 = 2003/80 & d_4 = 1521/40 \\
\delta_1 = 499/1716 & \delta_2 = 5/396 & \delta_3 = 801/1430 & \delta_4 = 17/26 \\
\rho_1 = 380/1573 & \rho_2 = 760/4719 & \rho_3 = 4776/7865 & \rho_4 = 280/1573 \\
\rho_5 = 12/143 & \rho_6 = 620/429 & \rho_7 = 504/715 & \rho_8 = 240/143 \\
\rho_9 = 1296/3575 & \rho_{10} = 72/1859 & &
\end{array}
\tag{31}
$$

References

[1] E.N. Lorenz. J. Atm. Sci. **20** (1963), 130-141.

[2] C. Boldrighini, V. Franceschini. Commun. Math. Phys. **64**, 159-170 (1979).

[3] Jie Shien. *Hopf Bifurcation of the Unsteady Regularized Driven Cavity Flow.* J. Comput. Phys. **95**, 228-245 (1991).

[4] Jie Shien. Comput. Methods Appl. Mech. Eng. **80**, 273 (1990).

[5] R. Temam. *Infinite Dimensional Dynamical Systems in Mechanics and Physics.* Springer-Verlag. New York (1988).

[6] R. Peyret, T.D. Taylor. *Computational Methods for Fluid Flow.* Springer-Verlag. (Springer Series in Computational Physics) (1983).

[7] C. Canuto, M.Y. Hussaini, A. Quarteroni, T.A. Zang. *Spectral Methods in Fluid Dynamics.* Springer-Verlag (Springer Series in Computational Physics) (1988).

[8] R.D. Moser, P. Moin, A. Leonard. *A spectral numerical method for the Navier-Stokes equations with applications to Taylor-Couette Flow.* J. Comput. Phys. **52**, 524-544 (1983).

[9] H.B.Keller. *Numerical Solution of bifurcation and nonlinear eigenvalue problems* in Applications of Bifurcation Theory, edited by P.H. Rabinowitz. Academic, New York, 1977.

[10] I. Shimada, T. Nagashima. Prog. Theor. Phys. **61** (1979), 1605-1615.

[11] M. Kubicek, M. Marek. *Computational Methods in Bifurcation Theory and Dissipative Structures.* Springer-Verlag (Springer Series in Computational Physics) (1983).

[12] D. Farmer, J.P. Crutchfield, H. Froehling, N.H. Packard, R. Shaw. Ann. N.Y. Acad. Sci. **357** (1980), 453. Part I (1981).